ORNL/TM-2018/1035

Evaluation of Zircaloy-4 Welding and Hydrogen Charging Effects for Use as the Structural Material for the Target Solution Vessel and Support Lines of SHINE

Lauren Garrison
Chinthaka Silva
Brian Eckhart
Chris Bryan

October 2018

OAK RIDGE NATIONAL LABORATORY
MANAGED BY UT-BATTELLE FOR THE US DEPARTMENT OF ENERGY

ORNL/TM-2018/1035

Material Science and Technology Division

EVALUATION OF ZIRCALOY-4 AS THE STRUCTURAL MATERIAL FOR THE TARGET SOLUTION VESSEL AND SUPPORT LINES OF SHINE—SAMPLE PREPARATION FOR THE THIRD-ROUND NEUTRON IRRADIATION

Lauren Garrison
Chinthaka Silva
Brian Eckhart
Chris Brian

Date Published: October 2018

Prepared by
OAK RIDGE NATIONAL LABORATORY
Oak Ridge, TN 37831-6283
managed by
UT-BATTELLE, LLC
for the
US DEPARTMENT OF ENERGY
under contract DE-AC05-00OR22725

CONTENTS

LIST OF FIGURES

LIST OF TABLES

ACKNOWLEDGMENTS

Support for this research was provided by the US Department of Energy's National Nuclear Security Administration (DOE/NNSA), Office of Material Management and Minimization, Molybdenum-99 Program. The authors would also like to thank the following coworkers for their contributions to completing this research project: Elizabeth Lindquist, Benjamin Gregory, Tyler Ray, Nesrin Cetiner, Wilna Geringer, Keith Leonard, Doug Stringfield, Deborah Counce, Kathy Jones, and Carol Lin.

1. INTRODUCTION

The subcritical hybrid intense neutron emitter (SHINE) is a proposed ^{99}Mo production facility to be constructed in the United States. It uses a deuterium (D) and tritium (T) fusion source to cause subcritical fission in an aqueous uranium solution, which is cycled to collect the ^{99}Mo products. The target solution vessel (TSV) is the container of the aqueous uranium solution, so it must remain structurally sound during operational exposure to water, fission products, neutrons, and hydrogen isotopes. The TSV will be large enough to require welding, so the exposure of joints to these same conditions must also be considered. The candidate material being investigated is Zircaloy-4. While Zircaloy-4 has a long history in the nuclear industry, it has primarily been used as fuel cladding at service temperatures of ~300°C. Zircaloy-4 must be evaluated for behavior under neutron irradiation at SHINE-relevant temperatures of <100°C. In this project, the effects of hydrogen, welding, and neutron irradiation at low temperatures are investigated.

2. EXPERIMENTAL DETAILS

2.1 MATERIAL INFORMATION

Zircaloy-4 material was procured from ATI Specialty Alloys and Components, in Oregon, USA. The material was from batch no. MIL-1526608 and had been hot rolled, annealed, blasted, and pickled by the supplier. The annealing was done at 782±14°C for 105 min, which is in the alpha phase temperature zone for Zircaloy-4. The Zircaloy-4 composition is Zr, 1.54 Sn, 0.21 Fe, and 0.11 Cr in wt %. It had a measured impurity of 0.14 wt % O, and ppm levels of other impurities of Al, C, N, Si, and H.

Tensile samples of SS3 geometry (Figure 1) were cut with the tensile direction parallel to the rolling direction of the Zircaloy-4 plate. This sample geometry has a total length of 25.4 mm (1 in.) and relies on shoulder contact between the sample and the tensile fixture to apply the load. There are no holes in the tab regions so that the tab material can be used for additional tests, including microhardness and microstructure analysis. This approach minimizes the material that must be neutron irradiated. The welding sample blocks (6×1.1×0.25 in.) were machined so that the welding seam was perpendicular to the rolling direction (Figure 2). The tungsten inert gas (TIG) welding was performed by Major Tool and Machine Inc. (Figure 3).

Then, the tensile samples were cut from the welded blocks so that their tensile direction was parallel to the rolling direction of the original Zircaloy-4 plate. Two versions of samples were machined (Figure 4). One was symmetric to the weld (SW) with the welded zone in the center gauge section of the tensile bar and the tabs on either side of the weld seam. The other type was asymmetric to the weld (BW) and had one tab in the weld and one tab in the base metal. These two sample types were chosen to explore the effect of stress on the weld, heat-affected zone, and base metal separately. Where the fracture was, compared with these three areas, gives information about which is the weak link of the material.

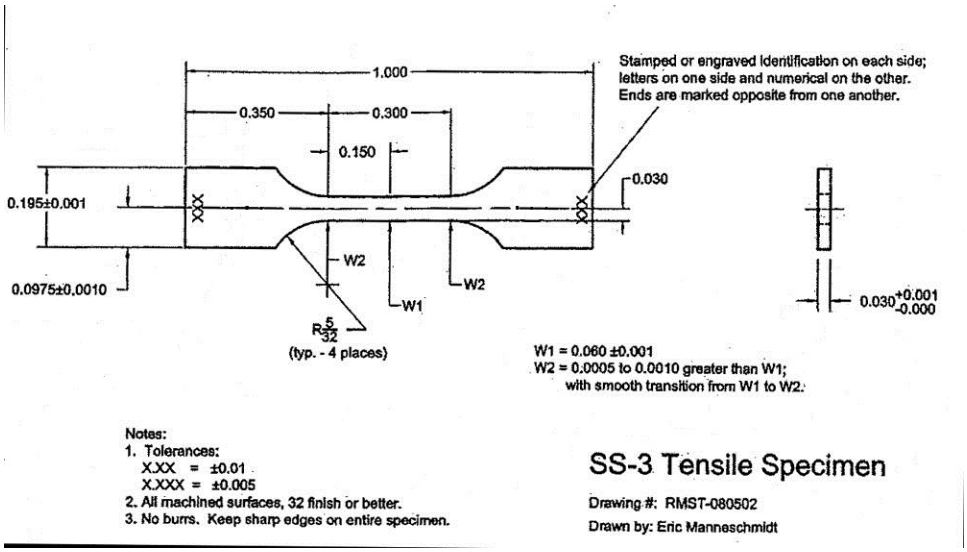

Figure 1. Drawing of the SS-3 tensile sample geometry, dimensions in inches.

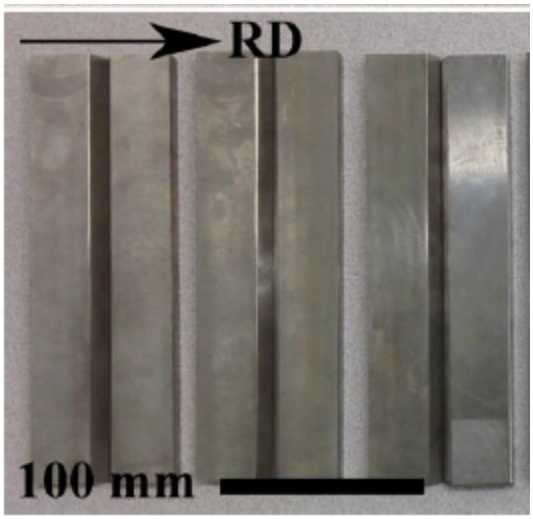

Figure 2. Cut bars of Zircaloy-4 for welding trials. The rolling direction (RD) of the original plate is indicated.

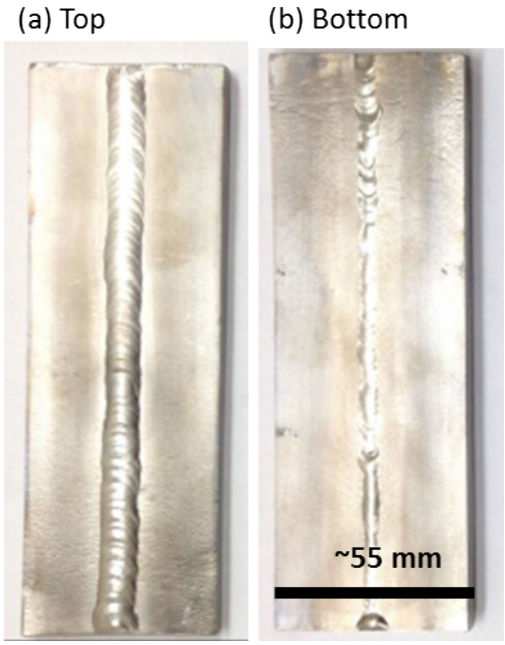

Figure 3. Example of welded test bar. For orientation specification, the wider side of the weld is referred to as the top and the opposite side as the bottom.

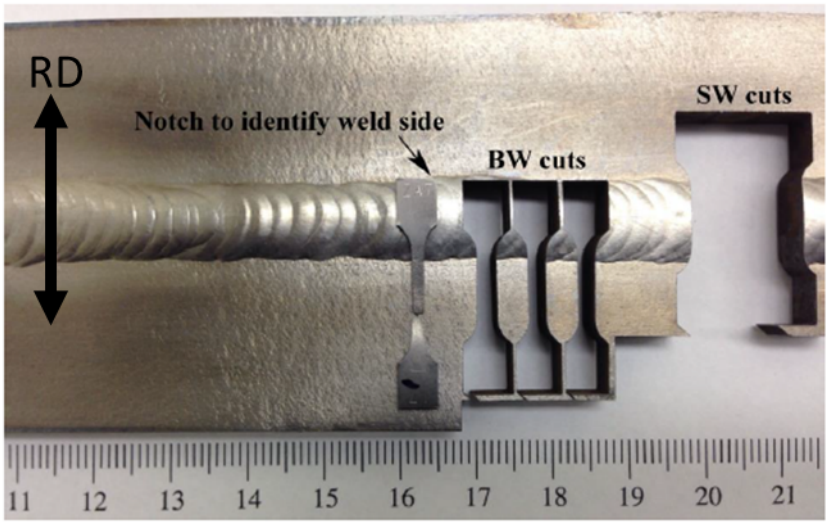

Figure 4. Example of symmetric tensile sample cut (SW) and asymmetric tensile sample cut (BW). Top side of the weld is shown.

2.2 X-RAY

X-ray images of the TIG-welded Zry-4 material were needed to show any large defects in the material and to select areas of interest for the tensile bar sample preparation. All the images were acquired using a Comet x-ray head unit with a single exposure of 30 seconds. The evaluated material had a thickness of 0.25 in.; therefore, the radiographs were acquired using 120/130 kV with 13 mA and a focal spot source

size of 5.5 mm. The images were captured using a source-to-film distance of 18, with a minimum source-to-object distance of ~ 17.5 in., and the source side-to-film distance used was ~0.5.

2.3 TENSILE

The tensile tests were performed at room temperature and atmospheric pressure in air on the SS-3 type samples. The majority of samples were tested at an extension rate of 0.0003 in./s, and selected samples were tested at 0.001 in./s to test the sensitivity to strain rate. Extensometers were not used for these tests, so the crosshead motion was recorded to estimate the strain of the samples. This method adds error to the measurement because of the machine compliance. The artifacts of machine compliance in the data can effectively be removed by analyzing the data to remove the elastic region. It is known that machine compliance adds error to the elastic region and apparent elastic slope of the tensile test, but that the stress values and plastic deformation are accurate for the sample material behavior.

The starting data form is the list of i points of engineering stress, σ_i, and raw engineering strain, ϵ_{raw_i}. Removing the effect of machine compliance on the data starts with determining the apparent elastic region slope, m. Then, Eq. (1) is used to calculate the plastic deformation, ϵ_{p_i} for all points in the series.

$$\epsilon_{p\_i} = \epsilon_{raw\_i} - \epsilon_o - \frac{\sigma_i}{m}. \quad (1)$$

In Eq. (1), ϵ_o is a static shift to the left or right that is applied to all the data so that it starts at (0, 0). Thus, after the transformation, the set of x-y points of σ_i versus ϵ_{p_i} were plotted and used to determine ultimate tensile strength (UTS), yield stress (YS), uniform elongation (UE), and total elongation (TE). An example of this data analysis and the transformation is shown in Figure 5. Equation (1) does not change the stress values; this is also illustrated in Figure 5, which shows that the UTS and YS before and after analyzing the data with Eq. (1) are identical. The data analysis allows the accurate UE and TE to be calculated, which are always less than the apparent elongations in the raw data.

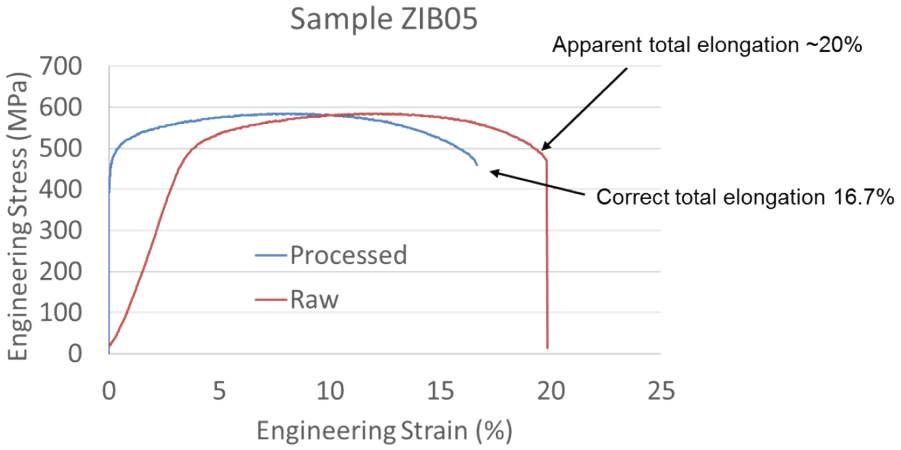

Figure 5. Example of tensile data analysis of sample ZIB05.

2.4 MICROHARDNESS

Microhardness testing was completed using a FM-700 instrument from Future-Tech Corp. Vickers hardness indenter was used with 10 s dwell time and varying indent loads. The Vickers hardness measurement uses a square-based pyramid that has 136° face angles. The hardness value was calculated

by the instrument using the applied force (F), average diagonal length of the indent (d), and Eq. (1) from Ref. [1]. For each case, five or more indents were completed, and their hardness values were averaged with the standard deviation of the set of measurements used as the uncertainty.

$$HV = 0.1891\frac{F}{d^2}\,. \tag{1}$$

2.5 HYDROGEN CHARGING

In a reactor environment, the largest source of hydrogen is the corrosion of zirconium by water, as in Eq. (2) from Ref. [2]. The hydrogen liberated from the water in the corrosion reaction has a high likelihood of being absorbed in the Zircaloy.

$$Zr + 2H_2O \rightarrow ZrO_2 + 2H_2 \tag{2}$$

Radiolysis of water by the neutrons is a second source of hydrogen that may be absorbed by the Zircaloy. Also, for the SHINE system, there are hydrogen isotopes in the gas phase in the accelerator system. While the accelerator system is separated from the TSV, this source of hydrogen may be considered for interaction with the Zircaloy-4 in off-normal or accident type scenarios.

Historically, the motivation of developing the Zircaloy-4 alloy was to reduce the hydrogen uptake compared with Zircaloy-2. This was accomplished by removing the nickel from Zircaloy-4 while leaving the rest of the alloying elements essentially the same between the two materials [2, 3]. As an example of the effect of this small change in alloy composition, Figure 6 shows the markedly reduced hydrogen absorption of Zircaloy-4 versus Zircaloy-2.

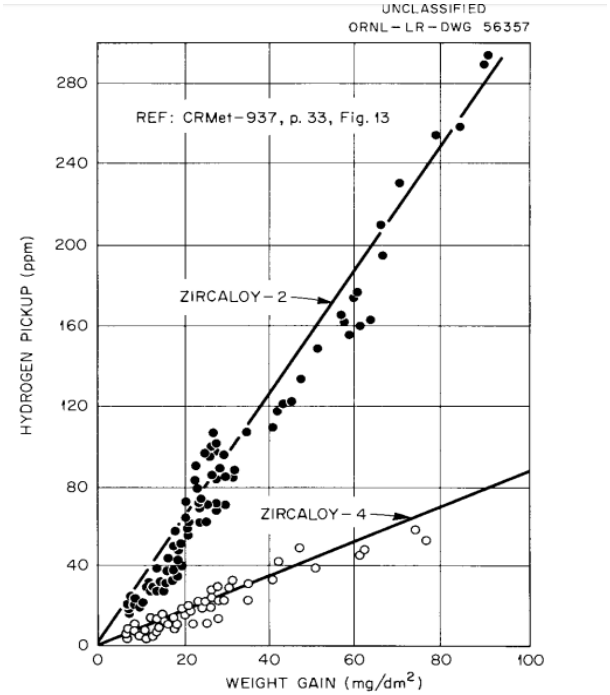

Figure 6. Example of lower hydrogen absorption in Zircaloy-4 as compared with Zircaloy-2. Reproduced from Ref. [2].

Hydrogen in Zircaloy is known to make the material more brittle, and this can be a point of failure. Additionally, there is less data on hydrogen interaction in Zircaloy-4, and particularly a lack of data for the low-temperature neutron irradiation conditions of the SHINE TSV. Thus, hydrogen charging to controlled amounts of hydrogen was completed on the base metal and welded material. The same method as in Ref. [4] was used, except that a smaller glass tube was used. Previously, the larger glass tube had to be connected to a smaller-diameter glass tube to pull the vacuum. These was a time-consuming two-step process. By loading the samples directly in the smaller diameter glass tube, it removes one of the joints and allows the vacuum to be pulled directly on the glass tube containing the sample and the Ni foil with the TiH_2 powder.

3. RESULTS AND DISCUSSION

3.1 X-RAY IMAGING

X-ray radiography was performed on the final batch of welded bars, labeled bars 10–13, from Major Tool and Machine. A Zry penetrameter (shim thickness 0.016 in.) with prescribed holes was used, as can be seen in Figure 7 with marker #5. This was used as a reference to the porosity of the holes in the x-ray images. The x-ray radiographs indicate the areas with porosity, within the TIG-welded material. The porosity could have been caused from an impurity in or on the material during the welding process. The impurities will cause micro gas bubbles to form, leaving a small void in the weld. Material number 11, shown in Figure 7, indicates a lack of penetration (LOP). This can be the result of the welding stick material not fully melting or bonding to the Zry-4 material. A slightly faster welding speed rate, or the height distance of the welding stick from the material, could have caused the lack of penetration. As shown in the x-ray radiographs, both the root pass and cover pass were fairly consistent throughout the welding passes. The result was that no significant voids or cracks were associated with either the root pass or cover pass.

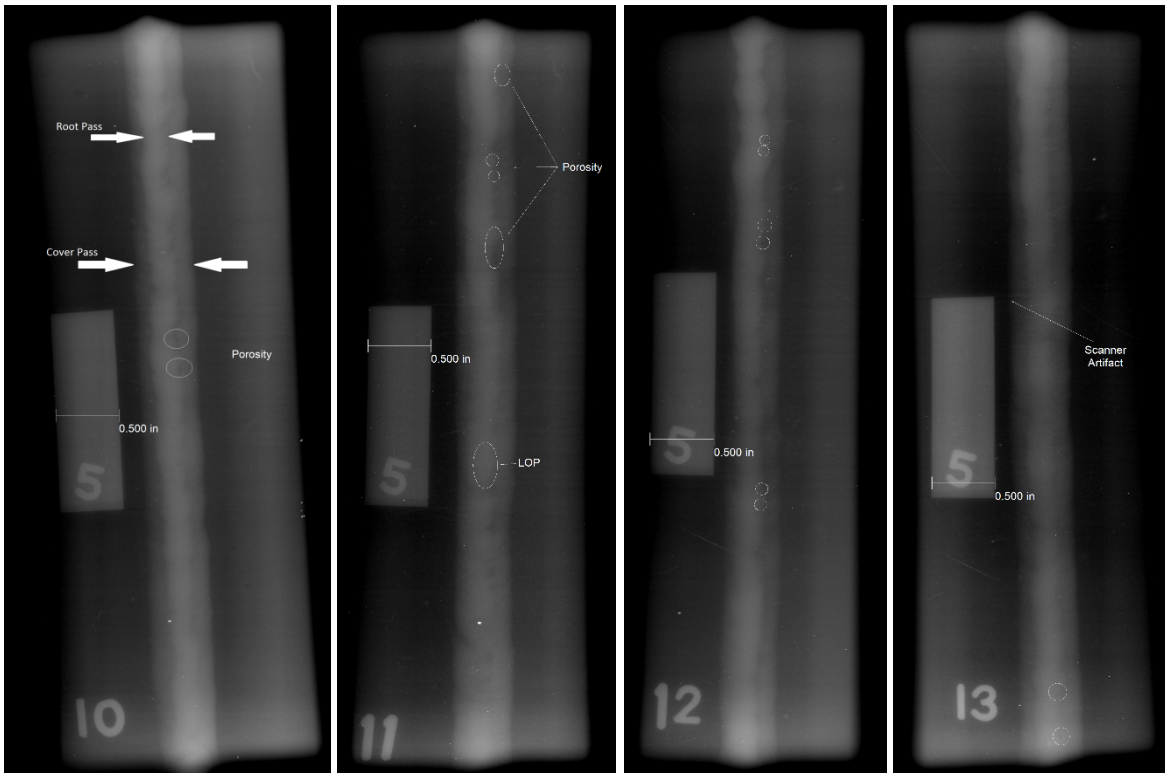

Figure 7 Four x-ray radiographs of TIG-welded Zry-4 material.

3.2 TENSILE

All values of strain discussed here have been adjusted with Eq. (1) to remove the artifacts from the testing method. The base metal tested samples had TE in the range of 22–29%. After welding, the BW type samples had TE similar to the base metal and were not severely affected by the weld. The SW type samples had TE in the range of 10–13%, so were more noticeably showing the effects of the weld. To recover the base metal properties, several post-weld heat treatments were performed. Part of the investigation was a series of post-weld heat treatments with 1 h holds at each of 500, 600, 700, 750, and 800°C [4].

Of these conditions, the 800°C case had slightly longer TE than the others so a further test of post-weld heat treatments at 800°C and different hold times was conducted. In the previous report Ref. [4], the tensile data were presented in raw form. Now, they have been analyzed using the method in Eq. (1) and are shown in

Table 1. The main difference from the previously reported raw data is the corrected TE values here. The largest average TE from these tests is 16.5% and is for the samples held for 1 hour at 800°C. Previously, the 1 hour hold time was identified as promising, based on tensile samples ZFE01-ZFE03, so additional samples ZIB06-ZIB09 were tested at the same condition. While the first set of ZFE01-ZFE03 had TE in the range of 16.71–18.55%, the set ZIB06-ZIB09 had TE in the range of 13.54–18.2%, bringing the overall average to 16.5%. This range of a few percentage points of TE variation was observed for several sample conditions previously and may be attributed to small differences between samples, such as how close to or far from the top of the welded bar the sample was cut. Depending on the depth in the welded bar, the sample would have a larger or smaller width of weld filler material in its gauge section, which can change the tensile properties.

The standard deviation of the TE was highest for the samples held for 24 hours at 800°C. It was observed previously that the large scatter in the TE for the long hold time samples was caused by extremely large grain growth that resulted in weak points in the material [4].

Table 1. Tensile results of post-weld heat treatments at 800°C and varying hold times. All samples were tensile tested at an extension rate of 0.0003 in/sec.

Sample	Weld type	Temp (C)	Hold time (h)	UTS (MPa)	YS (MPa)	UE (%)	TE (%)	Std. dev. TE (%)
ZFE01	SW	800	1	478.87	578.15	7.48	18.55	
ZFE02	SW	800	1	490.61	591.65	8.25	18.07	
ZFE03	SW	800	1	486.22	582.9	7.59	16.71	
ZIB06	SW	800	1	506.37	571.76	5.72	13.54	
ZIB07	SW	800	1	478.18	586.3	7.88	16.8	
ZIB08	SW	800	1	478.12	593.1	7.71	18.2	
ZIB09	SW	800	1	484.68	585.12	6.39	13.62	
			Averages	486.15	584.14	7.29	16.50	1.95
ZGA01	SW	800	12	491.51	587.51	6.83	15.14	
ZGA02	SW	800	12	492.96	582.17	6.04	13.74	
ZGA03	SW	800	12	483.2	583.83	7.23	14.09	
ZGA04	SW	800	12	479.66	571.59	5.9	13.92	
			Averages	486.83	581.28	6.5	14.22	0.54
ZGD01	SW	800	18	483.05	573.03	6.97	13.33	
ZGD02	SW	800	18	477.77	574.75	8.45	14.2	
ZGD03	SW	800	18	480.77	579.4	7.61	16.69	
			Averages	480.53	575.73	7.68	14.74	1.42
ZGB01	SW	800	24	480.72	580.61	10.62	22.05	
ZGB03	SW	800	24	487.25	552.68	4.27	11.49	
ZGB04	SW	800	24	426.47	466.18	2.1	8.16	
ZGB05	SW	800	24	486.43	593.5	7.38	16.48	
ZGB10	SW	800	24	402.97	470.92	2.24	9.06	
ZGB11	SW	800	24	387.84	437.37	3.21	8.62	
ZGB12	SW	800	24	401.36	453.81	2.8	7.63	
			Averages	439.01	507.87	4.66	11.93	5.00
ZGC01	SW	800	48	345.65	350.73	9.2	17.53	
ZGC02	SW	800	48	358.13	366.2	4.64	10.71	
ZGC03	SW	800	48	349.5	351.79	5.97	13.59	
ZGC04	SW	800	48	434.64	494.82	6.21	12.81	
			Averages	371.98	390.89	6.51	13.66	2.47

The strain sensitivity of the material was also tested by using two different extension rates of 0.0003 in./s and 0.001 in./s. Several samples were tested at each extension rate, and no important difference was observed in the tensile results (

Table 2). The TEs measured for both sets were within one standard deviation of each other, 15.75±2.12% and 16.50±1.95%. An example comparison between two samples tested at the different rates is shown in Figure 8, and the similarity is clear.

Table 2. Extension rate comparison for welded and heat-treated samples.

Sample ID	Weld type	Temp (°C)	Time (h)	extension rate	YS (MPa)	UTS (MPa)	UE (%)	TE (%)	Std. dev. TE (%)
ZHA02	SW	800	1	0.001 in/sec	477.1	575.26	6.19	15.17	
ZHA03	SW	800	1	0.001 in/sec	474.5	577.61	6.21	14.65	
ZHA04	SW	800	1	0.001 in/sec	486.28	600.83	7.63	16.11	
ZHA05	SW	800	1	0.001 in/sec	466.06	562.37	6.35	14.63	
ZIB01	SW	800	1	0.001 in/sec	473.63	552.99	6.17	17.12	
ZIB02	SW	800	1	0.001 in/sec	503.29	593.32	6.92	12.99	
ZIB03	SW	800	1	0.001 in/sec	499.85	601.76	7.51	20.62	
ZIB04	SW	800	1	0.001 in/sec	493.44	598.48	7.58	13.84	
ZIB05	SW	800	1	0.001 in/sec	488.82	594.49	7.72	16.66	
				Averages	484.77	584.12	6.92	15.75	2.12
ZIB06	SW	800	1	0.0003 in/sec	506.37	571.76	5.72	13.54	
ZIB07	SW	800	1	0.0003 in/sec	478.18	586.3	7.88	16.8	
ZIB08	SW	800	1	0.0003 in/sec	478.12	593.1	7.71	18.2	
ZIB09	SW	800	1	0.0003 in/sec	484.68	585.12	6.39	13.62	
ZFE01	SW	800	1	0.0003 in/sec	478.87	578.15	7.48	18.55	
ZFE02	SW	800	1	0.0003 in/sec	490.61	591.65	8.25	18.07	
ZFE03	SW	800	1	0.0003 in/sec	486.22	582.9	7.59	16.71	
				Averages	486.15	584.14	7.29	16.50	1.95

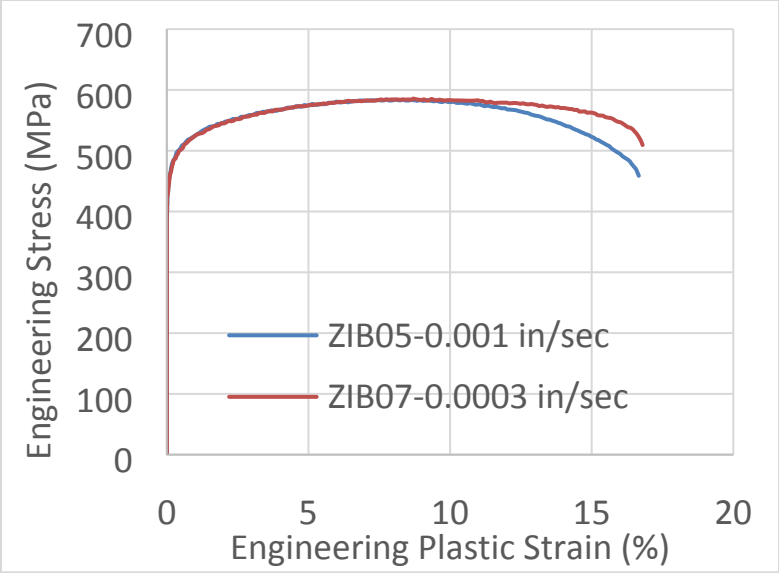

Figure 8. Samples tested at two extension rates had similar tensile results.

3.3 MICROHARDNESS

To determine the proper testing load, a series of microhardness tests with varying loads and 10 s dwell times were completed (Figure 9). From this analysis, it was determined that the microhardness plateaued at approximately 200–210 Hv for load values of 200 gf and higher. For lower loads, the microhardness calculated was artificially high. For the following tests, a load of 200 gf was used.

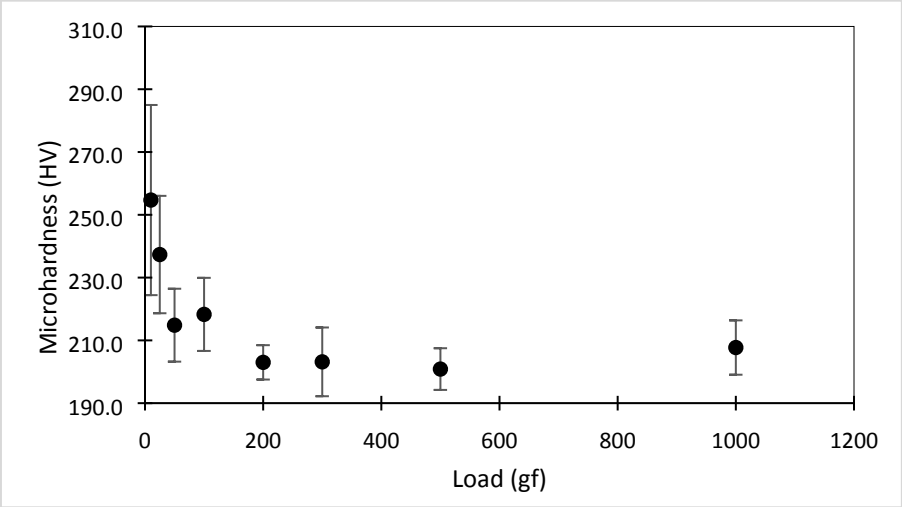

Figure 9. Microhardness indents were completed at varying loads and 10 s dwell time on a base metal Zircaloy-4 sample.

Sample Z01 was hydrogen charged to 100 wppm H and then microhardness tested. The hardness values varied from one tab end to the other in the range of 199.2±13.5 to 218.3±10.5 Hv. This is in the same range measured for the base metal nonhydrided sample. This low amount of hydrogen charging does not appear to affect the microhardness in a noticeable way. Hardness tests will be performed on samples charged with higher amounts of hydrogen.

Sample ZAT22 was an asymmetrically cut welded sample with no hydrogen charging and no post-weld heat treatment. This sample was tensile tested to fracture and then was microhardness indented along the length of the tensile axis from one tab to the other, in small steps on the order of 0.3 mm. Each data point in Figure 10 is one indent. Although this sample was cut asymmetrically to the weld, there was no significant difference from one tab end to the other in terms of the microhardness values. As the indents approached the tensile fracture, the microhardness increased slightly. The two points very close to the ends of the halves of the tensile sample (next to the dotted line) likely had some real increased hardness because they were in the area that was most plastically deformed; but these indents also were so close to the edge that they were difficult to measure, so the hardness values had very large uncertainties.

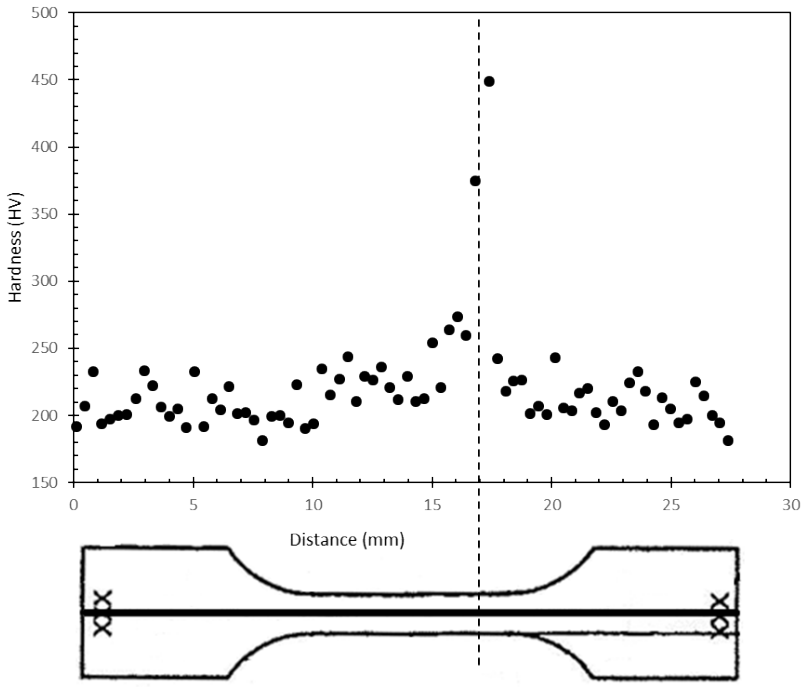

Figure 10. Sample ZAT22 microhardness tested along the tensile axis after tensile fracture. Dotted line indicates fracture point of tensile sample. Tensile sample drawing included for approximate scale guide to indents along the tensile axis.

3.4 HYDROGEN CHARGING

The first hydrogen charging experiment with the smaller glass tube was completed (Figure 11). Base metal sample Z29 was encased in the glass vacuum-sealed tube with 0.0047g of TiH_2 powder and a goal hydrogen charging amount of 500 wppm H. Based on the weight measurement after the hydriding, the sample retained 789 wppm H. The Leco gas analyzer system is being calibrated. Once that is completed, a more accurate measure of the retained hydrogen and any impurity oxygen will be measured with the Leco.

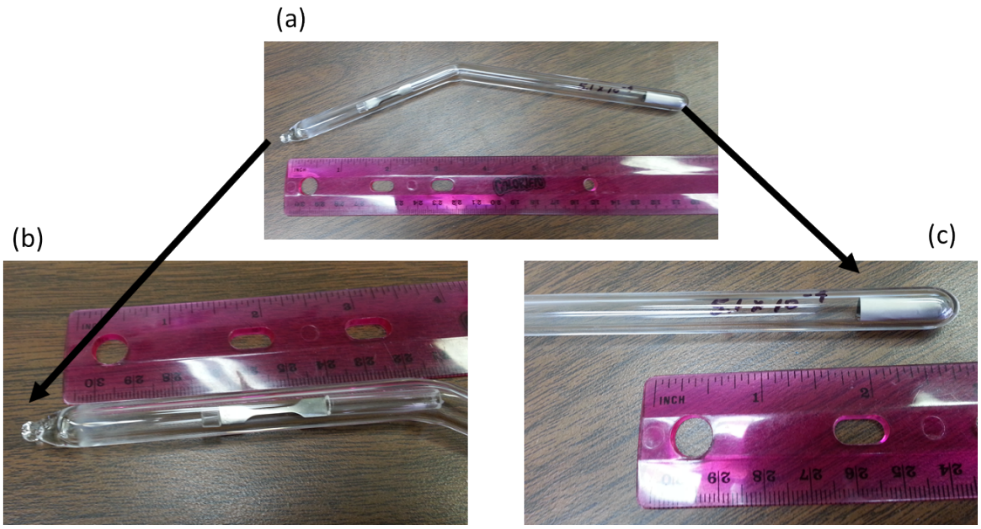

Figure 11. Hydriding test (a) in small glass tube, with (a) close-up of tensile bar with smaller glass spacer tube on either side to prevent shifting, and (c) close-up of the opposite end, which contains TiH_2 powder in a Ni foil.

4. FUTURE WORK

Samples of base metal, welded metal, and post-weld heat treated metal, all with and without hydrogen charging, are being prepared. These will be neutron irradiated in the High Flux Isotope Reactor at Oak Ridge National Laboratory at temperatures of 60 and 100°C and fluences of 1×10^{20} and 1×10^{21} n/cm^2 (E>0.1 MeV). Post-irradiation analysis will include tensile tests, microhardness, and microstructure analysis.

5. REFERENCES

[1] Future-Tech Corp, Digital Microhardness Tester Instruction and Maintenance Manual,
[2] C.L. Whitmarsh, Review of Zircaloy-2 and Zircaloy-4 properties relevant to N.S. Savannah reactor design, Oak Ridge National Laboratory, ORNL-3281, (1962).
[3] Reactor grade zirconium alloys for nuclear waste disposal-technical data sheet, ATI Wah Chang, www.alleghenytechnologies.com/wahchang, (2003).
[4] C. Silva, C. Bryan, Evaluation of Zircaloy-4 as the structural material for the Target Solution Vessel and support lines of SHINE — Sample preparation for the third-round neutron irradiation, Oak Ridge National Laboratory, ORNL/TM-2017/482, (2017).